

# A Nonlinear Position Controller for Maritime Operations of Rotary-wing UAVs

Xilin Yang, Matt Garratt and Hemanshu Pota

*School of Engineering and Information Technology  
University of New South Wales  
at the Australian Defence Force Academy, ACT, 2600, Australia  
e-mail: {x.yang, m.garratt, h.pota}@adfa.edu.au*

---

**Abstract:** This paper presents a disturbance attenuation controller for horizontal position stabilization for hover and automatic landings of a Rotary-wing Unmanned Aerial Vehicle (RUAV) operating in rough seas. Based on a helicopter model representing aerodynamics during the landing phase, a nonlinear state feedback  $\mathcal{H}_\infty$  controller is designed to achieve rapid horizontal position tracking in a gusty environment. The resultant control variables are further treated in consideration of practical constraints (flapping dynamics, servo dynamics and time lag effect) for implementation purpose. The high-fidelity closed-loop simulation using parameters of the Vario helicopter verifies performance of the proposed position controller. It not only increases the disturbance attenuation capability of the RUAV, but also enables rapid position response when gusts occur. Comparative studies show that the  $\mathcal{H}_\infty$  controller exhibits great performance improvement and can be applied to ship/RUAV landing systems.

*Keywords:* Helicopter control, Helicopter dynamics,  $\mathcal{H}_\infty$  control

---

## 1. INTRODUCTION

RUAVs are suitable for a variety of applications such as surveillance and reconnaissance, search and rescue, and scientific investigations. There is also a growing desire to operate a RUAV from ships at sea which introduces new challenges owing to adverse turbulence over the flight deck and ship motion through waves. Operational flexibility, including vertical take-off and landing capability, hover at a desired height, longitudinal and lateral manoeuvre, makes the RUAV an indispensable platform to perform maritime operations.

The main challenge in fulfilling maritime landing tasks results from the complicated aerodynamic environment, which consists of wave-excited movement of the ship deck and turbulent gusts. The RUAV operates in a partial ground effect condition where both the magnitude of the rotor flow and the inflow distribution over the rotor disk vary greatly (Xin et al., 2001). This phenomenon results in a considerable change in the aerodynamic loading of the rotor system, which may affect the RUAV control margins, autopilot workload and power margins (Toffoletto et al., 2002). Therefore, dynamic performance of the RUAV is deteriorated and pure feedback driven controllers fail to stabilize the position response. This difficulty justifies the need for a controller with gust-attenuation properties. In addition, for an automatic landing, the descent trajectory of the RUAV deviates greatly from the desired trajectory when strong gusts occur. This necessitates rapid and accurate tracking performance to avoid missing the landing deck. Therefore, fast position response is another requirement for the controller design to achieve a safe landing.

Investigation of helicopter control in a turbulent environment has received attention in some papers. Cheviron et al. (Cheviron et al., 2009) proposed a robust guidance and control scheme for an autonomous helicopter in the presence of wind gusts. Martini et al. (Martini et al., 2008) addressed control of a model-scale helicopter under wind gusts. The disturbances in their paper were purely vertical wind gusts with typical levels less than  $1\text{ms}^{-1}$ . Robust control of helicopters has also been discussed in a number of papers. Civita et al. (Civita et al., 2006) succeeded in implementing an  $\mathcal{H}_\infty$  loop-shaping controller on a Yamaha R-50 helicopter. It was reported that tracking performance was improved using this design approach. Other papers related to robust control of helicopters can be found in Ref. (Kung, 2008).

The present research is part of efforts devoted to developing a feasible procedure for landing a RUAV on moving platforms in typical sea states. Our objective is to design a controller with a disturbance attenuation property and rapid horizontal position tracking performance. This work begins with establishing a simplified model capturing dynamics of the RUAV during landing operations. Afterwards, a nonlinear  $\mathcal{H}_\infty$  controller is developed to achieve gust attenuation and fast horizontal position control. Simulation results demonstrate that the proposed controller can effectively attenuate gust effects and achieve rapid and accurate position tracking when gusts occur.

## 2. A NONLINEAR $\mathcal{H}_\infty$ POSITION CONTROLLER

### 2.1 Modeling of Helicopter Dynamics

In the considered application, height of the RUAV can be stabilized in a gusty environment using the proportional-

derivative (PD) controller with a feedforward compensator (Yang et al., 2009). Control of the yaw motion can also be achieved by the existing PD controller. Therefore, in this paper, particular emphasis is placed on a more challenging task of rapid control of RUAV planar positions in the presence of wind gusts, and the control objective is to design a disturbance attenuation controller for the RUAV to track the desired horizontal trajectory to fulfil a safe and reliable landing.

The design of a disturbance attenuation controller depends greatly on the choice of typical working conditions expected and tractability of the control problem associated with the resultant control plants. Normally, hover state is a typical working condition, and stabilization of the hover state is a prerequisite for an automatic landing. Therefore, the control plant will be derived for the hover condition, where main rotor thrust  $T_{mr}$  and tail rotor thrust  $T_{tr}$  are constant. A complete helicopter dynamic model can be found in Ref. (Padfield, 2007), and it can be reduced to the following forms for controller design,

$$\dot{x}_b = u + d_1 \quad (1)$$

$$\dot{y}_b = v + d_2 \quad (2)$$

$$\dot{u} = r_c v - q w_c + \frac{X_h}{M_a} - g\theta + d_3 \quad (3)$$

$$\dot{v} = -r_c u + p w_c + \frac{Y_h}{M_a} + g(\phi + \phi_0) + d_4 \quad (4)$$

$$\dot{p} = k_1 p q + k_2 q r_c + k_3 L_h + k_4 N_h + d_5 \quad (5)$$

$$\dot{q} = k_5 p r_c + k_6 (r_c^2 - p^2) + k_7 M_h + d_6 \quad (6)$$

$$\dot{\phi} = p + (q(\phi + \phi_0) + r_c)\theta + d_7 \quad (7)$$

$$\dot{\theta} = q - r_c(\phi + \phi_0) + d_8 \quad (8)$$

Here,  $(x_b, y_b)$  are horizontal positions.  $(u, v, w_c)$  and  $(p, q, r_c)$  are linear and angular velocities with the subscript  $c$  indicating that the yaw rate  $r_c$  and vertical velocity  $w_c$  are obtained from onboard sensors (inertial measurement unit and GPS). Control inputs are longitudinal flapping  $a_1$  and lateral flapping  $b_1$ , disturbance input is  $d_{(\cdot)}$ . The roll and pitch are denoted by  $\phi$  and  $\theta$ . The parameters  $k_{(\cdot)}$  are listed as follows

$$\begin{aligned} \xi &= I_{xx} I_{zz} - I_{xz}^2 & k_1 &= \frac{I_{xz}(I_{xx} - I_{yy} + I_{zz})}{\xi} \\ k_2 &= \frac{I_{zz}(I_{yy} - I_{zz}) - I_{xz}^2}{\xi} & k_3 &= \frac{I_{zz}}{\xi} \\ k_4 &= \frac{I_{xz}}{\xi} & k_5 &= \frac{I_{zz} - I_{xx}}{I_{yy}} \\ k_6 &= \frac{I_{xz}}{I_{yy}} & k_7 &= \frac{1}{I_{yy}} \end{aligned}$$

where  $I_{xx}, I_{yy}, I_{zz}$  and  $I_{xz}$  are moments of inertia and product of inertia. External forces  $(X_h, Y_h, Z_h)$  and moments  $(L_h, M_h, N_h)$  acting on the RUAV take the form of

$$L_h = k_\beta b_1 + T_{mr} D_{mz} b_1 + T_{tr} D_{tz} \quad (9)$$

$$M_h = (-k_\beta - T_{mr} D_{mz}) a_1 \quad (10)$$

$$N_h = \frac{P_{mr}}{\Omega} + T_{mr} D_{mx} b_1 + T_{tr} D_{tx} \quad (11)$$

where  $k_\beta$  is the center-spring rotor stiffness, and geometry parameters of the Vario helicopter  $D_{mz}, D_{tz}, D_{mx}$  and  $D_{tx}$  are listed in Table 1.

The main rotor flapping dynamics are described by

Table 1. Parameters of the Vario helicopter

Parameters	Value
$a_{mr}$ : Main rotor blade 2D lift curve slope	5.7
$a_{tr}$ : Tail rotor blade 2D lift curve slope	4.0
$A_l$ : Lateral cyclic to main rotor pitch ratio	-0.17 rad/ms
$B_l$ : Longitudinal cyclic to main rotor pitch ratio	-0.19 rad/ms
$C_l$ : Longitudinal cyclic to flybar pitch ratio	-1.58 rad/ms
$D_l$ : Lateral cyclic to flybar pitch ratio	-1.02 rad/ms
$c_{mr}$ : Main rotor blade chord	0.076 m
$c_{tr}$ : Tail rotor blade chord	0.043 m
$D_{mx}$ : Horizontal distance between main rotor and $y$ -axis	0.036 m
$D_{my}$ : Sideways distance between main rotor and $x$ -axis	-0.0029 m
$D_{mz}$ : Vertical distance between main rotor and horizontal plane	-0.3321 m
$D_{tx}$ : Horizontal distance between tail rotor and $y$ -axis	-1.4440 m
$D_{ty}$ : Sideways distance between tail rotor and $x$ -axis	-0.0029 m
$D_{tz}$ : Vertical distance between tail rotor and horizontal plane	1.1379 m
$I_{xx}$ : Moment of inertia about $x$ -axis	12.3 kgm <sup>2</sup>
$I_{yy}$ : Moment of inertia about $y$ -axis	18.7 kgm <sup>2</sup>
$I_{zz}$ : Moment of inertia about $z$ -axis	6.6 kgm <sup>2</sup>
$I_{xz}$ : Product of inertia	0
$K_s$ : Flybar to main rotor pitch mixing ratio	0.8
$k_\beta$ : center-spring rotor stiffness	1165.7 N/m
$M_a$ : All-up weight	27.738 kg
$N_b$ : Number of main rotor blades	3
$R_b$ : Main rotor radius	1.25 m
$S_{fus}^X$ : Fuselage equivalent flat plate area in $x$ -direction	-0.036 m <sup>2</sup>
$S_{fus}^Y$ : Fuselage equivalent flat plate area in $y$ -direction	0.0029 m <sup>2</sup>
$S_{fus}^Z$ : Fuselage equivalent flat plate area in $z$ -direction	-0.6379 m <sup>2</sup>
$\Omega$ : Main rotor angular velocity	89.01 rad/sec
$\Omega_{tr}$ : Tail rotor angular velocity	481.55 rad/sec

$$\dot{a}_1 = -q - \frac{a_1}{\tau_f} + \frac{1}{\tau_f} \left( \frac{\partial a}{\partial u} u + A_{lon} \delta_{lon} \right) \quad (12)$$

$$\dot{b}_1 = -p - \frac{b_1}{\tau_f} + \frac{1}{\tau_f} \left( \frac{\partial b}{\partial v} v + B_{lat} \delta_{lat} \right) \quad (13)$$

where  $\tau_f = \frac{16}{\gamma\Omega}$  is main rotor time constant with  $\gamma$  denoting the lock number and  $\Omega$  the main rotor angular speed.  $A_{lon}$  and  $B_{lat}$  are effective steady-state longitudinal and lateral gains,  $\delta_{lon}$  and  $\delta_{lat}$  are longitudinal cyclic and lateral cyclic. The Dihedral effect is

$$\frac{\partial a}{\partial u} = -\frac{\partial b}{\partial v} = \frac{2}{\Omega R} \left( \frac{8C_T}{\alpha\sigma} + \sqrt{\frac{C_T}{2}} \right) \quad (14)$$

where  $R$  is main rotor radius,  $\alpha$  life curve slope,  $\sigma$  the solidity ratio, and  $C_T$  thrust coefficient.

*Remark 1.* Adoption of existing controllers for vertical (feedback-feedforward controller) and yaw motion (PD controller) makes it possible to treat  $T_{mr}$  and  $T_{tr}$  as constant. Thus, update equations for  $\dot{z}_b, \dot{w}_c$  and  $\dot{r}_c$  are neglected.

*Remark 2.* The constant offset  $\phi_0$  is added to the system dynamics to establish the desired equilibrium point for rolling motion. This enables zero initial condition and facilitates the control design.

*Remark 3.* The RUAV attitudes are very small ( $\phi, \phi_0, \theta, \psi < 5^\circ$ ). Using small angle approximation, the simplified trigonometric functions are

$$\begin{aligned}\sin \theta &\approx \theta \quad \cos \theta \approx 1 \quad \tan \theta \approx \theta \\ \sin(\phi + \phi_0) &\approx \phi + \phi_0 \quad \cos(\phi + \phi_0) \approx 1\end{aligned}$$

*Remark 4.* For model-scale helicopters, control forces and moments are mainly generated by main rotor and tail rotor. Forces and moments from fuselage, empennage and vertical fin are neglected.

*Remark 5.* Control inputs in the controller design process are set to be longitudinal flapping and lateral flapping. They will be converted later into longitudinal cyclic and lateral cyclic for implementation.

The following vectors are defined,

$$\begin{aligned}x &= [x_b, y_b, u, v, p, q, \phi, \theta]^T \\ \omega &= [d_1, d_2, d_3, d_4, d_5, d_6, d_7, d_8]^T \\ U_c &= [a_1, b_1]^T\end{aligned}$$

which lead to a compact form of system dynamics

$$\dot{x} = f(x) + g_1(x)\omega + g_2(x)U_c \quad (15)$$

$$\dot{z}_m = h(x) + l(x)U_c \quad (16)$$

Here,  $x \in \mathbf{R}^8$  is plant state,  $\omega \in \mathbf{R}^8$  disturbance, and  $U_c \in \mathbf{R}^2$  control input.  $z_m \in \mathbf{R}^{10}$  is a penalty variable. It is assumed that all functions involved are smooth and defined in a neighborhood  $U_e$  of the origin in  $\mathbf{R}^8$  and  $f(0) = 0$ ,  $h(0) = 0$ . The following assumptions are also made,

$$\begin{aligned}h^T(x)l(x) &= 0 \\ l^T(x)l(x) &= R_h\end{aligned} \quad (17)$$

where  $R_h \in \mathbf{R}^{2 \times 2}$  is a nonsingular constant matrix, and is chosen to be symmetric to facilitate controller design.

The design approach is based on the theory proposed in Ref. (Isidori and Astolfi, 1992; Khalaf et al., 2006) with modifications necessitated by RUAV aerodynamics. The control objective is to design a controller  $U_c = L(x)$  to achieve satisfactory closed-loop system performance evaluated either in time domain (overshoot, steady-state error and settling time etc.) or in frequency domain (magnitude and phase margin). It is expected that the initial state departing in the vicinity of the equilibrium point converges to the equilibrium point when time goes to infinity. The disturbance attenuation capability can be described as (Isidori and Astolfi, 1992): Give a real number  $0 < \gamma_h < 1$ , it is said that the exogenous signals are locally attenuated by  $\gamma_h$  if there exists a neighborhood  $U_e$  of the point  $x = 0$  such that for every  $T > 0$  and for every piecewise continuous function  $\omega : [0, T]$ , the state trajectory starting from  $x_0 = 0$  remains in  $U_e$  for all  $t \in [0, T]$ , and the response  $z_m : [0, T]$  satisfies

$$\int_0^T z_m^T(s)z_m(s)ds \leq \gamma_h^2 \int_0^T \omega^T(s)\omega(s)ds \quad (18)$$

The design approach begins with Taylor series expansion of the nonlinear functions in Eq. (15)-(16),

$$f(x) = \sum_{i=1}^{\infty} A_i x^{(i)} = A_1 x + f^{[2+]}(x) \quad (19)$$

$$h(x) = \sum_{i=1}^{\infty} C_i x^{(i)} = C_1 x + h^{[2+]}(x) \quad (20)$$

$$g_1(x) = B_1 + g_1^{[1+]}(x) \quad (21)$$

$$g_2(x) = B_2 + g_2^{[1+]}(x) \quad (22)$$

where  $f^{[2+]}(x), h^{[2+]}(x), g_1^{[1+]}(x)$  and  $g_2^{[1+]}(x)$  are high-order expansions.

For the RUAV model Eq.(1)-(8),  $f(x)$  has a third-order expansion, and the three terms  $A_1, A_2$  and  $A_3$  are written as follows

$$A_1 = \begin{bmatrix} 0 & 0 & 1 & 0 & 0 & 0 & 0 & 0 \\ 0 & 0 & 0 & 1 & 0 & 0 & 0 & 0 \\ 0 & 0 & 0 & r_c & 0 & -w_c & 0 & -g \\ 0 & 0 & -r_c & 0 & w_c & 0 & g & 0 \\ 0 & 0 & 0 & 0 & k_1 q & k_1 p + k_2 r_c & 0 & 0 \\ 0 & 0 & 0 & 0 & k_5 r_c - 2k_6 p & 0 & 0 & 0 \\ 0 & 0 & 0 & 0 & 1 & (\phi + \phi_0)\theta & q\theta & q(\phi + \phi_0) \\ 0 & 0 & 0 & 0 & 0 & 1 & -r_c & 0 \end{bmatrix}_{8 \times 8}$$

where  $A_2 \in \mathbf{R}^{8 \times 64}$  and  $A_3 \in \mathbf{R}^{8 \times 512}$  are large sparse matrices with a small number of non-zero values. The non-zero elements with their indices are listed below

$$\begin{aligned}A_2(5, 38) &= k_1 & A_2(5, 45) &= k_1 \\ A_2(6, 37) &= -2k_6 & A_2(7, 47) &= \theta \\ A_2(7, 48) &= \phi + \phi_0 & A_2(7, 54) &= \theta \\ A_2(7, 56) &= q & A_2(7, 62) &= \phi + \phi_0 \\ A_2(7, 63) &= q \\ A_3(7, 376) &= 1 & A_3(7, 383) &= 1 \\ A_3(7, 432) &= 1 & A_3(7, 446) &= 1 \\ A_3(7, 495) &= 1 & A_3(7, 502) &= 1\end{aligned}$$

and  $A_i = 0$  for  $i > 3$ .

The functions  $g_1(x)$  and  $g_2(x)$  can be expanded to the first-order,

$$B_1 = B_1^0 = [B_{11}, \dots, B_{18}] = I_8 \quad (23)$$

$$B_2 = B_2^0 = [B_{21}, B_{22}] \quad (24)$$

where

$$B_{21} = \begin{bmatrix} 0 & 0 & \frac{T_{mr}}{M_a} & 0 & 0 & b_1 & 0 & 0 \end{bmatrix}^T \quad (25)$$

$$B_{22} = \begin{bmatrix} 0 & 0 & 0 & \frac{T_{mr}}{M_a} & b_2 & 0 & 0 & 0 \end{bmatrix}^T \quad (26)$$

with

$$\begin{aligned}b_1 &= k_7(-k_\beta - T_{mr}D_{mz}) \\ b_2 &= k_3 k_\beta + k_3 T_{mr}D_{mz} + k_4 T_{mr}D_{mx}\end{aligned}$$

The constant matrices  $h(x)$  and  $l(x)$  are given by the expressions

$$h(x) = \begin{bmatrix} x_1 & & & & & & & \\ & \delta x_2 & & & & & & \\ & & \ddots & & & & & \\ & & & \delta x_8 & & & & \\ \hline 0 & \dots & \dots & 0 & & & & \\ 0 & \dots & \dots & 0 & & & & \end{bmatrix}_{10 \times 8} \quad l(x) = \begin{bmatrix} O_{8 \times 2} \\ I_2 \end{bmatrix}_{10 \times 2} \quad (27)$$

where  $\delta$  is a non-negative real number for making the controller design trade-off.

### 2.2 Linear Part of the $\mathcal{H}_\infty$ Controller

The linear part of the  $\mathcal{H}_\infty$  controller can be obtained after solving the algebraic Riccati equation described by

$$H_{px}^T \bar{P} + \bar{P} H_{px} + \bar{P} H_{pp} \bar{P} x + H_{xx} = 0 \quad (28)$$

with the following definitions

$$H_{px} = A_1 \quad H_{xx} = C_1^T C_1 \quad H_{pp} = \frac{B_1 B_1^T}{\gamma_h^2} - B_2 R_h^{-1} B_2^T \quad (29)$$

The solution  $\bar{P}$  is required to construct the controller.

Eq. (28) can be rearranged into standard  $\mathcal{H}_\infty$ -like Riccati Equation form ( $R_h = I_2$ )

$$A_1^T \bar{P} + \bar{P} A_1 - \bar{P} \begin{bmatrix} B_1 & B_2 \end{bmatrix} \begin{bmatrix} -\gamma_h^2 I_{m_1} & O_{m_1 \times m_2} \\ O_{m_2 \times m_1} & I_{m_2} \end{bmatrix}^{-1} \begin{bmatrix} B_1^T \\ B_2^T \end{bmatrix} \bar{P} + C_1^T C_1 = 0 \quad (30)$$

where  $m_1 = 8, m_2 = 2$  and  $\gamma_h$  is the attenuation factor. It can be obtained that the system is both controllable and observable, and the unique positive semi-definite matrix  $\bar{P}$  exists.

### 2.3 Nonlinear Part of the $\mathcal{H}_\infty$ Controller

**Notation and Definitions** The following manipulations are introduced

$$x^{(0)} = 1 \quad x^{(1)} = x \quad x^{(i)} = \underbrace{x \otimes x \otimes \dots \otimes x}_{i \text{ factor}}, \quad i = 2, 3, \dots \quad (31)$$

where  $\otimes$  is the Kronecker product. It is also defined that

$$x^{[0]} = 1 \quad x^{[1]} = x, \quad x^{[k]} = [x_1^k, x_1^{k-1} x_2, \dots, x_1^{k-2} x_2^2, x_1^{k-2} x_2 x_3, \dots, x_n^k]^T, \quad k \geq 1 \quad (32)$$

Constant matrices  $M_k$  and  $N_k$  can be used to set up the relationship between  $x^{(k)}$  and  $x^{[k]}$

$$x^{[k]} = M_k x^{(k)} \quad x^{(k)} = N_k x^{[k]} \quad (33)$$

where  $M_k \in \mathbf{R}^{C(n_x, k) \times n_x^k}$  and  $N_k \in \mathbf{R}^{n_x^k \times C(n_x, k)}$  satisfy

$$M_k N_k = I_{n_x}^{[k]} \quad (34)$$

Here,  $I_{n_x}^{[k]}$  is an identity matrix of dimension

$$C(n_x, k) := C_{n_x+k-1}^k = \frac{\prod_{i=1}^k (n_x + k - i)}{k!} \quad (35)$$

The number of states is  $n_x = 8$ .

We adopt the following operator  $row(A)$  which maps  $n$  by  $m$  matrix  $A = (a)_{ij}$  to a 1 by  $mn$  row vector

$$row(A) = [a_{11}, a_{12}, \dots, a_{1m}, \dots, a_{n1}, \dots, a_{nm}] \quad (36)$$

Also, for any integers  $i \geq 1, k \geq i$ , and row vector  $\bar{P}_k^*$  of dimension  $n_x^k$ , there exists a matrix  $\bar{P}_k^i \in \mathbf{R}^{n_x \times n_x^{k-i}}$  determined by  $\bar{P}_k^*$  such that

$$\bar{P}_k^*(x^{(i-1)} \otimes I_{n_x} \otimes x^{(k-i)}) = (\bar{P}_k^i x^{(k-1)})^T \quad (37)$$

where  $\bar{P}_k^*$  is partitioned to a 1 by  $n_x^i$  block matrix taking the form

$$\bar{P}_k^* = \left[ \underbrace{P_{1 \dots 11}}_{i \text{ tuple}} \dots \underbrace{P_{1 \dots 1n_x}}_{i \text{ tuple}} \dots \underbrace{P_{n_x \dots n_x 1}}_{i \text{ tuple}} \underbrace{P_{n_x \dots n_x n_x}}_{i \text{ tuple}} \right] \quad (38)$$

in which  $P_{j_1, \dots, j_i}, 1 \leq j_1, \dots, j_i \leq n_x$  is a row vector of dimension  $n_x^{k-i}$ . The resultant matrix  $\bar{P}_k^i$  is given by

$$\bar{P}_k^i = \begin{bmatrix} \underbrace{P_{1 \dots 11}}_{i \text{ tuple}} & \underbrace{P_{1 \dots 21}}_{i \text{ tuple}} & \dots & \underbrace{P_{n_x \dots n_x 1}}_{i \text{ tuple}} \\ \underbrace{P_{1 \dots 12}}_{i \text{ tuple}} & \underbrace{P_{1 \dots 22}}_{i \text{ tuple}} & \dots & \underbrace{P_{n_x \dots n_x 2}}_{i \text{ tuple}} \\ \vdots & \vdots & \vdots & \vdots \\ \underbrace{P_{1 \dots 1n_x}}_{i \text{ tuple}} & \underbrace{P_{1 \dots 2n_x}}_{i \text{ tuple}} & \dots & \underbrace{P_{n_x \dots n_x n_x}}_{i \text{ tuple}} \end{bmatrix}$$

The controller design process is as follows (Khalaf et al., 2006). Let  $S_2 = \bar{P}$ , and the following intermediate matrices are computed

$$W_{ij}^2 = row(S_2 B_{ij}^1); \quad i = 1, 2; j = 1, \dots, 8 \quad (39)$$

$$Y_{11}^1 = B_{11}^T S_2^T = B_{11}^T \bar{P}; \quad E_3 = row(\bar{P} A_2) \quad (40)$$

$$F_3 = \sum_{l=1}^2 (C_l^T C_{3-l}) = 0 \quad I_3^1 = \sum_{l=2}^2 \sum_{j=1}^8 row((W_{1j}^1)^T Y_{1j}^{3-l}) \quad (41)$$

$$I_3^2 = \sum_{j=1}^2 row((W_{2j}^2)^T Y_{2j}^1) \quad (42)$$

Then,

$$H_3 = -(E_3 + \frac{F_3 - 2I_3^2}{2} + \frac{I_3^1}{\gamma_h^2}) N_3 = -E_3 N_3 \quad (43)$$

$$M_3 = x^{[3]} (x^{(3)})^{-1} \quad N_3 = x^{(3)} (x^{[3]})^{-1} \quad (44)$$

Also, the intermediate matrix  $U_3$  is

$$U_3 = M_3 \left[ \sum_{i=1}^3 I_8^{(i-1)} \otimes \bar{T} \otimes I_8^{(3-i)} \right] N_3 \quad (45)$$

$$= M_3 [\bar{T} \otimes I_8^{(2)} + I_8^{(1)} \otimes \bar{T} \otimes I_8^{(1)} + I_8^{(2)} \otimes \bar{T}] N_3 \quad (46)$$

where  $\bar{T} = H_{px} + H_{pp} \bar{P}$ . Then

$$\bar{P}_3 = H_3 U_3^{-1} \quad \bar{P}_3^* = \bar{P}_3 M_3 \quad S_3 = \sum_{i=1}^3 (\bar{P}_3^i)^T \in \mathbf{R}^{64 \times 8} \quad (47)$$

The next step is to compute  $\bar{P}_4$ , which is  $\bar{P}_4 = H_4 U_4^{-1}$ . The following intermediate matrices are calculated

$$E_4 = \sum_{l=2}^3 row(S_l A_{5-l}) \quad F_4 = \sum_{l=1}^3 row(C_l^T C_{4-l}) = 0 \quad (48)$$

$$Z_4 = row(S_3 H_{pp} S_3^T) \quad W_{ij}^3 = \sum_{l=2}^3 row(S_l B_{ij}^{4-l}); \quad (49)$$

$$I_4^1 = \sum_{l=2}^3 \sum_{j=1}^8 row((W_{1j}^1)^T Y_{1j}^{4-l}) \quad G_4^1 = \sum_{l=2}^2 \sum_{j=1}^8 row((W_{1j}^1)^T W_{ij}^{4-l}) \quad (50)$$

$$I_4^2 = \sum_{l=2}^3 \sum_{j=1}^2 row((W_{2j}^2)^T Y_{2j}^{4-l}) \quad G_4^2 = \sum_{j=1}^8 row((W_{2j}^2)^T W_{2j}^2) \quad (51)$$

$$M_4 = x^{[4]} (x^{(4)})^{-1} \quad N_4 = x^{(4)} (x^{[4]})^{-1} \quad (52)$$

Afterwards,  $H_4 = -\frac{1}{2}(Z_4 + 2E_4)N_4$ .

The  $U_4$  can be computed as

$$U_4 = M_4 \left[ \sum_{i=1}^4 I_8^{(i-1)} \otimes \bar{T} \otimes I_8^{(4-i)} \right] N_4$$

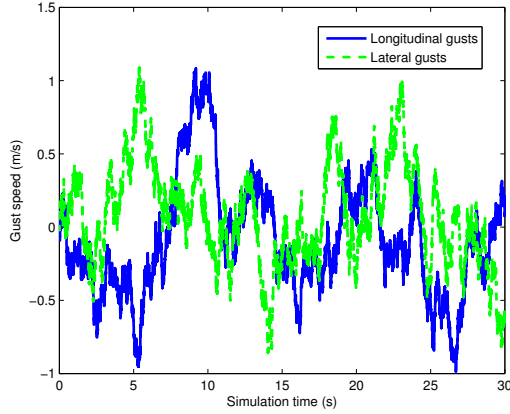


Fig. 1. Horizontal gusts used to test  $\mathcal{H}_\infty$  controller

Table 2. Control gains for PID controllers

	$k_p$	$k_i$	$k_d$
Altitude-PD	0.4	0	0.05
Yaw-PD	0.8	0	1.05
Roll-PD	-0.9	0	-0.5
Pitch-PD	0.5	0	0.1
Longitudinal-PD	-0.1	0	-0.1
Lateral-PID	0.05	0.005	0.2

$$= M_4[\bar{T} \otimes I_8^{(3)} + I_8^{(1)} \otimes \bar{T} \otimes I_8^{(2)} + I_8^{(2)} \otimes \bar{T} \otimes I_8^{(1)} + I_8^{(3)} \bar{T}] N_4$$

Afterwards,

$$\bar{P}_4 = H_4 U_4^{-1} \quad \bar{P}_4^* = \bar{P}_4 M_4 \quad S_4 = \sum_{i=1}^4 (\bar{P}_4^i)^T \in \mathbf{R}^{512 \times 8} \quad (53)$$

The  $\mathcal{H}_\infty$  controller takes the following form

$$U_c = (-R_h^{-1} B_2^T \bar{P})x + (-R_h^{-1} \begin{bmatrix} B_{21}^T S_3^T \\ B_{22}^T S_3^T \end{bmatrix} N_2)x^{[2]} \\ + (-R_h^{-1} \begin{bmatrix} B_{21}^T S_4^T \\ B_{22}^T S_4^T \end{bmatrix} N_3)x^{[3]} \quad (54)$$

The suggested controller satisfies disturbance attenuation property given in Eq. (18). For proof, interested readers can refer to (Khalaf et al., 2006).

### 3. SIMULATION RESULTS

#### 3.1 Performance Evaluation of the $\mathcal{H}_\infty$ Controller

In this section, performance of the  $\mathcal{H}_\infty$  controller is evaluated using parameters of the Vario helicopter shown in Table 1. To make the results more applicable, servo dynamics are taken into account. Also, synchronization assessment is performed by adding pure lag component into the closed-loop simulation.

The longitudinal and lateral flapping commands given in Eq. (54) need to be converted into longitudinal and lateral cyclic for implementation. As the flapping reacts instantaneously, the longitudinal and lateral cyclic can be calculated using a closed-form linear solution given the desired flapping angles  $a_1^{des}$  and  $b_1^{des}$  generated by the  $\mathcal{H}_\infty$  controller, i.e.,

$$\delta_{lon} = q\tau_f - a_1^{des} - \frac{\partial a}{\partial u} u; \quad \delta_{lat} = -p\tau_f - b_1^{des} + \frac{\partial b}{\partial v} v \quad (55)$$

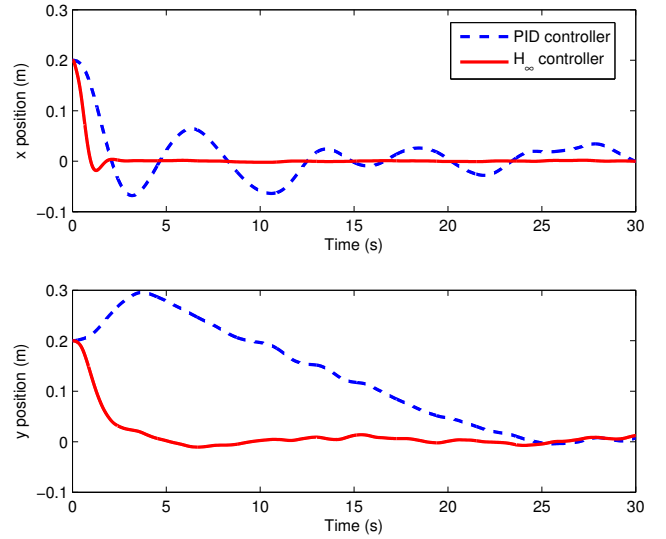


Fig. 2. Helicopter position response using PID controller and  $\mathcal{H}_\infty$  controller

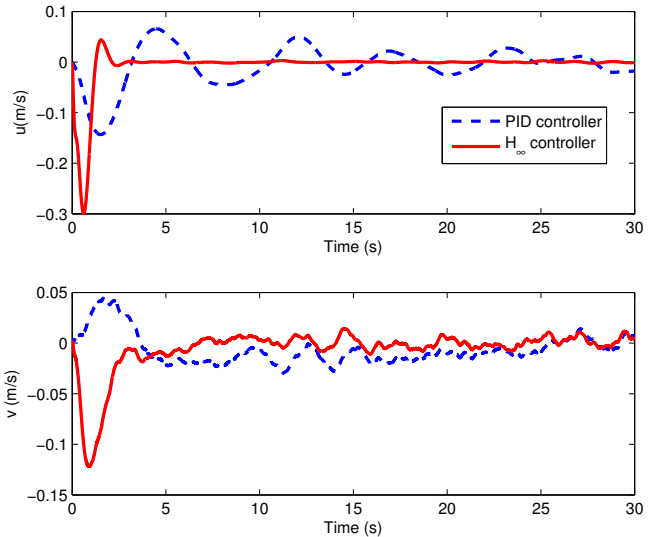


Fig. 3. Helicopter velocity response using PID controller and  $\mathcal{H}_\infty$  controller

It has been identified experimentally that servo dynamics can be approximated using the first-order transfer function with time constant  $\tau_s$  (Garratt, 2007; Ahmed et al., 2010). We tested the upper limit of  $\tau_s$  that the  $\mathcal{H}_\infty$  controller can tolerate. For Vario platform, simulations show that the upper limit turns out to be 60ms. In practice, performance of the controller is also affected by synchronization issue. This is essentially due to the fact that pure lags exist because sensor data arrive at different time. This is caused by transmitting, decoding and waiting until the next control update cycle. Therefore, a group of signals are required to wait for certain time in order to generate control commands in conjunction with other signals of late arrival. Pure lags are unavoidable when a controller is to be applied in practice. The simulations reveal that the  $\mathcal{H}_\infty$

controller can tolerate a pure lag up to 30ms. Although servo dynamics and pure lag effect are not considered when designing the  $\mathcal{H}_\infty$  controller, the upper bounds from the simulations provide a clue on the requirement of implementing our controller.

PID controllers have been widely applied due to their simplicity and effectiveness. In the considered application, height and yaw motion are stabilized using the feedforward and PD controllers. For the inner loop (roll and pitch) dynamics, two PD controllers are employed. Once control of inner loop is achieved, PID controllers are tuned for position and velocity (outer loop) control with the integral of the error signal eliminating undesired offsets.

The coupling effects between the inner loop and the outer loop of the helicopter dynamics make it challenging to tune PID control gains to achieve satisfactory responses. Simulations suggest that PID gains should be tuned separately. The strategy is to firstly tune control gains for altitude and yaw motion. Then, control of roll and pitch in the inner loop can be accomplished by repeating the same procedure. Afterwards, control gains in outer loop are tuned while control gains in inner loop are frozen. In the simulation, six PID controllers with the form

$$U_{PID} = k_p + \frac{k_i}{s} + k_d s \quad (56)$$

are selected with five PD controllers for altitude, yaw, roll, pitch and longitudinal position. A PID controller is used to remove offsets in lateral position.

To obtain the proper PID control gains, we empirically choose a group of gains which satisfy performance specifications such as settling time ( $< 40s$ ) and steady-state error ( $< \%5$  of reference signal). The integral of squared errors

$$J_e = \int_0^T [e_z^2(t) + e_\psi^2(t) + e_\theta^2(t) + e_\phi^2(t)] dt + \int_0^T [e_x^2(t) + e_y^2(t)] dt$$

provides a principle to choose the proper control gains. Symbols  $e_z, e_\psi, e_\theta, e_\phi, e_x, e_y$  are attitude and position errors. The proper PID control gains are selected such that they can reduce  $J_e$  greatly while exhibiting satisfactory transient response. Table 2 lists the suitable gains for comparison purposes.

For the  $\mathcal{H}_\infty$  controller, exogenous disturbances are simulated using the *Dryden* gust model, as is show in Fig. 1. It is assumed that  $\delta = 0.2$  and attenuation factor  $\gamma_h = 6$ . It takes 35.9 seconds to compute the weighting matrices in the controller. The horizontal position responses are shown in Fig. 2. It is noticed that positions  $x_b$  and  $y_b$  settle faster to the desired values ( $x_b = 0, y_b = 0$ ) from initial positions ( $x_b = 0.2m, y_b = 0.2m$ ) when the  $\mathcal{H}_\infty$  controller is applied. The faster responses are the outcome of the rapid velocity responses depicted in Fig. 3. It takes more than 25s for the PID controller to attenuate gust effect to an acceptable level, and the oscillations in position cannot be damped completely.

#### 4. CONCLUSION AND FUTURE WORK

In this paper, a disturbance attenuation position controller is developed for RUAVs operating in a gusty environment. The horizontal positions are stabilized via a nonlinear state-feedback  $\mathcal{H}_\infty$  controller. Performance of the proposed controller is evaluated through simulations in consideration of servo dynamics and pure lags. Comparative

studies show that our controller can settle positions of the RUAV more rapidly than a PID controller in a gusty environment. Future work will focus on conducting flight tests of the  $\mathcal{H}_\infty$  controller on the Vario helicopter.

#### ACKNOWLEDGEMENTS

The authors would like to thank Dr. Hamid Teimoori Sangani and Mr. Peter Leichsenring for useful discussions.

#### REFERENCES

- Ahmed, B., Pota, H., and Garratt, M. (2010). Flight control of a rotary wing uav using backstepping. *International Journal of Robust and Nonlinear Control*, 20(6), 639–658.
- Chevion, T., Plestan, F., and Chriette, A. (2009). A robust guidance and control scheme of an autonomous scale helicopter in presence of wind gusts. *International Journal of Control*, 82(12), 2206–2220.
- Civita, M.L., Papageorgiou, G., Messner, W.C., and Kanade, T. (2006). Design and flight testing of an  $\mathcal{H}_\infty$  controller for a robotic helicopter. *Journal of Guidance, Control, and Navigation*, 29(2), 485494.
- Garratt, M.A. (2007). *Biologically Inspired Vision and Control for an Autonomous Flying Vehicle*. Ph.D. thesis, Australian National University, Australia.
- Isidori, A. and Astolfi, A. (1992). Disturbance attenuation and  $\mathcal{H}_\infty$ -control via measurement feedback in nonlinear systems. *IEEE transactions on automatic control*, 37(9), 1283–1293.
- Khalaf, M.A., Huang, J., and Lewis, F.L. (2006). *Nonlinear  $\mathcal{H}_2/\mathcal{H}_\infty$  Constrained Feedback Control: A Practical Design Approach Using Neural Networks (Advances in Industrial Control)*. Springer.
- Kung, C.C. (2008). Nonlinear  $\mathcal{H}_\infty$  robust control for six DOF equations of motion of rigid body with mass uncertainty. In *Proceedings of the 17th World Congress, the International Federation of Automatic Control*, 11346–11351.
- Martini, A., Leonard, F., and Abba, G. (2008). Dynamic modelling and stability analysis of model-scale helicopters under wind gust. *Journal of Intelligent and Robot Systems*, 54(4), 647–686.
- Padfield, G.D. (2007). *Helicopter Flight Dynamics: the Theory and Applications of Flying Qualities and Simulation Modelling, 2nd edition*. Blackwell Publishing.
- Toffoletto, R., Reddy, R., and Lewis, J. (2002). Effect of ship frontal shape variation on flow field in flight deck region. In *Proceedings of the 2nd International Conference on Computational Fluid Dynamics, ICCFD*. Sydney, Australia.
- Xin, H., He, C., and Lee, J. (2001). Combined finite state rotor wake and panel ship deck models for simulation of helicopter shipboard operations. In *the American Helicopter Society 57th Annual Forum*, 1187–1200. the American Helicopter Society International, Inc., Washington, DC.
- Yang, X., Pota, H., and Garratt, M. (2009). Design of a gust-attenuation controller for landing operations of unmanned autonomous helicopters. In *18th IEEE International Conference on Control Applications*, 1300–1305. Saint Petersburg, Russia.